Cellular Digital Post-Distortion: Signal Processing Methods and RF Measurements

Huseyin Babaroglu, Lauri Anttila, Guixian Xu, Matias Turunen, Markus Allén, and Mikko Valkama
Department of Electrical Engineering, Tampere University, Tampere, Finland

***Abstract*—In this paper, we study the feasibility of digital post-distortion (DPoD) based mitigation of transmitter nonlinear distortion in cellular networks. With specific emphasis on downlink, we describe a computationally efficient one-shot method to estimate and mitigate the cascaded multipath channel and transmitter nonlinear distortion effects at terminal receiver, building on demodulation reference symbols (DMRSs). We also describe a DMRS boosting approach to match the envelope characteristics of the DMRS and the actual data-bearing multicarrier symbols such that accurate mitigation is feasible. We provide RF measurement results with a state-of-the-art 28 GHz active antenna array and 256-QAM data modulation, demonstrating larger performance enhancements in received signal error vector magnitude (EVM) compared to existing computationally expensive iterative methods.**

***Index Terms*—5G, 6G, active array, digital post-distortion, energy-efficiency, nonlinear distortion, power amplifiers.**

I. Introduction

Trading between power-efficiency and transmit waveform quality is, in general, one of the most challenging implementation concerns in radio transmitters [1]. To this end, digital pre-distortion (DPD) [2] is the de-facto solution for mitigating power amplifier (PA) nonlinear distortion in cellular base-stations. However, future millimeter-wave (mmWave) networks with active antenna arrays and wide waveform bandwidths make adopting DPD increasingly complex [1]. This is due to the need of over-the-air (OTA) observation receivers and the very large processing rates.

Alternative to DPD, digital post-distortion (DPoD) [3] is a receiver (RX) based approach where the primary target is to enhance the received signal error vector magnitude (EVM), and thereon, to improve the bit or symbol detection. Such receiver based scheme does not help in transmitter out-of-band (OOB) emission concerns, however, as the radiated power at mmWaves is typically EVM limited [4], DPoD can offer means for improved network energy-efficiency when combined with relaxation of the transmitter side EVM requirements. This is currently a timely topic also in 3GPP 5G NR standardization [5] and is the main technical focus of this paper.

In the existing DPoD literature, Cioffi *et al.* [6] proposed an iterative approach, called power amplifier nonlinearity cancellation (PANC), to cancel the nonlinear distortion at the RX side. In [3], an iterative post-distortion detection approach, referred to as reconstruction of distorted signals (RODS), is proposed where nonlinear distortion terms are included in the signal detection. The work in [7], in turn, combines PANC algorithm with channel and nonlinear distortion estimation. Similarly, in [8], a combination of PANC with frequency- and time-domain channel estimation (FD-TD-PANC) is proposed. Finally, in [9], PANC with PA model parameter estimation and channel estimation is considered.

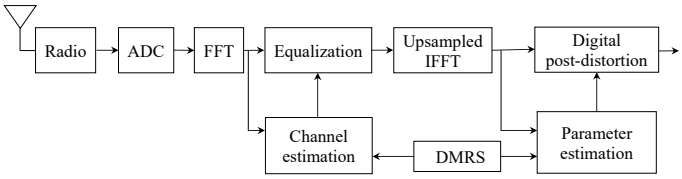

Fig. 1. Block diagram of the proposed DPoD scheme at the UE receiver to mitigate the nonlinear effects induced by the transmitter.

Specifically, adopting DPoD in cellular downlink calls for computationally feasible parameter estimation and distortion cancellation algorithms that can be executed in real-time at the user equipment (UE). To this end, in this paper, we describe a reduced complexity EVM enhancement method avoiding the iterative processing assumed in [3], [6]–[9]. Additionally, we build the parameter estimation of the cascaded transmitter nonlinearity and the multipath channel on the existing downlink demodulation reference symbols (DMRSs). This allows for tracking the mobile radio channel and the beam-dependent nonlinear distortion characteristics [1], [4] at millisecond level, or even faster depending on the network subcarrier spacing and slot length. Furthermore, we show that the DMRS bearing OFDM symbols have different envelope characteristics than the actual physical downlink shared channel (PDSCH) OFDM symbols, and describe a DMRS boosting approach such that nonlinear distortion estimation is feasible at receiver side. Finally, RF measurement results are provided using a state-of-the-art mmWave active phased-array transmitter operating at 28 GHz. The results show that the proposed DPoD approach can reach similar or improved performance compared to the iterative PANC method, despite the largely reduced real-time processing complexity. Especially with high data modulation orders such as 256-QAM and when the transmit signal is subject to strong nonlinear distortion, the proposed method outperforms PANC.

II. DPoD Methods

A. Received Signal Model

We start by shortly stating the received signal model under a nonlinear transmitter. First, at the transmitter (TX) side, the discrete-time OFDM signal is generated by applying the inverse fast Fourier transform (IFFT) to the M-QAM modulated data symbols, denoted by a_k at active subcarriers

$k \in \{-N_{\text{act}}/2, \ldots, N_{\text{act}}/2\}$. We assume that the subcarrier spacing is Δf and the sampling rate $f_s = \varepsilon N_{\text{FFT}} \Delta f$, where ε is the oversampling factor and N_{FFT} is the corresponding basic FFT size. Then, each OFDM symbol consists of $N = \varepsilon\, N_{\text{FFT}}$ time-domain samples, with a sample interval of $T_s = \frac{1}{N\Delta f}$. Then, by appending the cyclic prefix (CP) of length N_{CP}, the time-domain OFDM signal within an arbitrary multicarrier symbol duration can be expressed as

$$x(n) = \frac{1}{\sqrt{N}} \sum_{k=-N_{\text{act}}/2}^{N_{\text{act}}/2} a_k e^{j2\pi kn/N}, \quad -N_{\text{CP}} \leq n \leq N. \quad (1)$$

Next, for modeling the transmitter nonlinear distortion, we employ the widely-used memory polynomial (MP) model [10]. The corresponding nonlinearly distorted transmit waveform, $y(n)$, can be expressed as

$$y(n) = \sum_{\substack{p=1 \\ p \text{ odd}}}^{P_{\text{TX}}} \sum_{d=0}^{D_{\text{TX}}} c_{p,d} x(n-d)|x(n-d)|^{(p-1)}, \quad (2)$$

where $c_{p,d}$ represents the complex coefficient for p-th order and d-th delayed nonlinearity. We note that the model in (2) can, in general, model either the output of an individual PA unit or the effective beamformed output of an active antenna array – for further details refer, e.g., to [4].

Then, the transmit waveform propagates through a noisy multipath channel. We assume that the receiver basic sample rate is $f_{s,\text{RX}} = N_{\text{FFT}} \Delta f$, and that the UE front-end contains channel selection filtering. The corresponding channel filtered received signal is transformed at UE into frequency domain, via N_{FFT} point FFT. The resulting frequency-domain samples at active bins can be expressed in vector-matrix form as

$$\mathbf{R}(k) = \mathbf{H}(k)\mathbf{Y}_{\text{filt}}(k) + \mathbf{W}(k), \quad (3)$$

where $\mathbf{H}(k)$, $\mathbf{Y}_{\text{filt}}(k)$, and $\mathbf{W}(k)$ represent the FFTs of the channel impulse response, channel-filtered transmit waveform, and channel-filtered thermal noise, respectively.

B. Digital Post-Inverse Method

Next, we describe the proposed one-shot approach, called Digital Post-Inverse (DPoI), to mitigate the nonlinear passband effects of the transmitter – illustrated conceptually in Fig. 1. The actual DMRS-based estimation of the channel response as well as the nonlinear distortion parameters are described in the following subsection, while here we describe the fundamental processing with given parameter estimates.

First, normal linear equalization is applied to combat the channel linear distortion, expressed as

$$\mathbf{Q}(k) = \mathbf{H}_{\text{eq}}(k)\mathbf{H}(k)\mathbf{Y}_{\text{filt}}(k) + \mathbf{H}_{\text{eq}}(k)\mathbf{W}(k), \quad (4)$$

where $\mathbf{H}_{\text{eq}}(k)$ denotes the equalizer frequency response at the active bins. Then, to account for the TX nonlinearities, the signal is oversampled by a factor of ε and transformed back to time-domain. This can be achieved with proper bin stacking of $N = \varepsilon\, N_{\text{FFT}}$ sized IFFT, yielding a sample sequence of

$$q(n) = \tilde{y}(n) + \tilde{w}(n), \quad (5)$$

where $\tilde{y}(n)$ and $\tilde{w}(n)$ denote the upsampled time-domain sequences of the first and the second terms in (4).

The actual DPoD processing, reflecting a post-inverse, is next carried out in which we deploy a memory polynomial processing engine – similar to the transmitter nonlinearity modeling in (2). We express this as

$$\hat{x}(n) = \sum_{\substack{p=1 \\ p \text{ odd}}}^{P_{\text{RX}}} \sum_{d=0}^{D_{\text{RX}}} \tilde{c}_{p,d} q(n-d)|q(n-d)|^{(p-1)}, \quad (6)$$

where $\tilde{c}_{p,d}$ denote the MP model coefficients used in the UE processing. Finally, the output signal $\hat{x}(n)$ is decimated by ε, followed by N_{FFT} point FFT back to the subcarrier domain for the actual bit or symbol detection.

C. Parameter Estimation and DMRS Boosting

1) DMRS-based Parameter Estimation

Next, we address the actual DMRS-based estimation of the memory polynomial parameters. The linear channel estimation using the same DMRS is conceptually well-known, the linear minimun mean-squared error (LMMSE) estimator being one of the most established approaches [11]. For DPoI parameter estimation, we assume that the linear channel estimation is carried out first, and the corresponding received signal during the DMRS transmission is also equalized. This equalized signal can then be expressed similar to (6) but with known transmit sequence (the DMRS) as the source. To this end, by denoting the upsampled DMRS signal by $q_{\text{ref}}(n)$, the DPoD output during the DMRS symbol can be formally written as

$$x_{\text{ref}}(n) = \sum_{\substack{p=1 \\ p \text{ odd}}}^{P_{\text{RX}}} \sum_{d=0}^{D_{\text{RX}}} \tilde{c}_{p,d} q_{\text{ref}}(n-d)|q_{\text{ref}}(n-d)|^{(p-1)}. \quad (7)$$

Next, for notational convenience, we switch to vector matrix algebra. Let $\tilde{\boldsymbol{c}}$ represent the $(P_{\text{RX}}+1)(D_{\text{RX}}+1)/2 \times 1$ vector of complex nonlinear coefficients and $\boldsymbol{\Upsilon}$ the $N \times (P_{\text{RX}}+1)(D_{\text{RX}}+1)/2$ matrix of nonlinear basis function samples. Each column of $\boldsymbol{\Upsilon}$ is represented by $\Upsilon_{p,d}$ associated with a complex coefficient $\tilde{c}_{p,d}$, such that

$$\Upsilon_{p,d}(n) = q_{\text{ref}}(n-d)|q_{\text{ref}}(n-d)|^{p-1}. \quad (8)$$

Thus, (7) can be represented as $\boldsymbol{x}_{\text{ref}} = \boldsymbol{\Upsilon}\tilde{\boldsymbol{c}}$ where $\boldsymbol{x}_{\text{ref}}$ is an $N \times 1$ vector of received samples during the DMRS-bearing OFDM symbol. Finally, the unknown parameter vector $\tilde{\boldsymbol{c}}$ can be estimated with least-squares (LS) as

$$\tilde{\boldsymbol{c}} = (\boldsymbol{\Upsilon}^H \boldsymbol{\Upsilon})^{-1} \boldsymbol{\Upsilon}^H \boldsymbol{x}_{\text{ref}} \quad (9)$$

It is fair to note that as discussed, e.g., in [12], a noisy input in inverse model estimation will produce a bias in the coefficients. However, as our RF measurement based numerical results show, this approach still provides a good enhancement in receiver EVM performance.

2) DMRS Boosting

In the previous parameter estimation method, it is basically assumed that the DMRS-bearing OFDM symbol carries only the

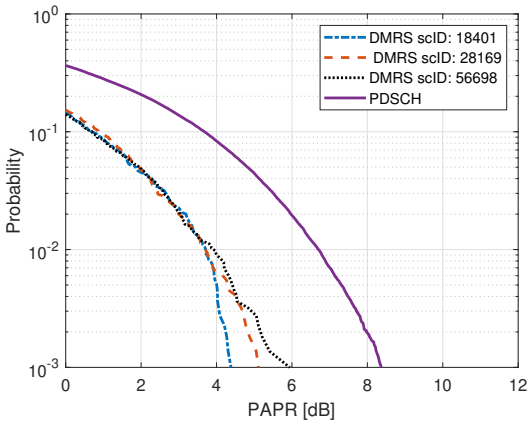

Fig. 2. PAPR complementary cumulative distribution functions (CCDFs) of PDSCH and DMRS OFDM symbols with different scrambling identities.

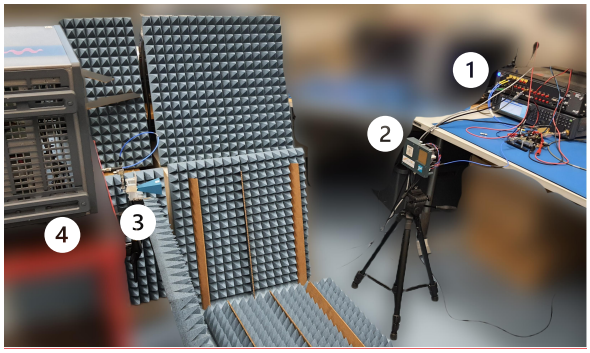

Fig. 3. 28 GHz OTA setup with active antenna array transmitter used in the FR2 measurements. (1) Transmitter chain, including AWG, mixer, image filter and driver amplifiers, (2) Anokiwave AWMF-0129 active antenna array, (3) Pasternack PE9851A-20 antenna, (4) Keysight UXR0402AP oscilloscope.

DMRS sequence with no data being frequency-multiplexed. This, however, results in different envelope characteristics compared to the actual data bearing PDSCH symbols. This is illustrated in Fig. 2, in terms of PAPR CCDFs. Such difference directly renders the DMRS based MP model estimate useless from the PDSCH point of view. Hence, we propose to boost the DMRS power such that the envelope characteristics are essentially matched. The results in Fig. 2 also illustrate that strictly speaking, different DMRS sequences have different PAPR tails, however, the probability for such is less than 1%, and is thus not a major issue in practice.

D. Complexity Analysis

The computational complexities of the proposed DPoI and the PANC [6] reference method are next assessed, in terms of real multiplications (*mul*) and real additions (*add*) per OFDM symbol. We assume that FFT/IFFT operations are performed with the radix-2 Cooley-Tukey algorithm, which requires $8N\log_2 N$ *mul*s and $6N\log_2 N$ *add*s for an N-point FFT/IFFT [13]. Furthermore, we assume that basis functions with $p \geq 3$ are obtained in a recursive manner using previous basis function, e.g., $\Upsilon_{5,0} = \Upsilon_{3,0}|q(n)|^2$. Basis functions with memory are simply generated via shifting, requiring thus no additional calculations. Furthermore, equalization, coefficient estimation, and final bit or symbol decoding are not included in the analysis since they are common in both methods.

DPoI is executed non-iteratively including IFFT/FFT, which requires $8N\log_2 N$ *mul*s and $6N\log_2 N$ *add*s, and post-distortion through (6), requiring $N(P{+}1)(2D{+}3)$ *mul*s and $N[2(P{+}1)(D{+}1){-}1]$ *add*s. In addition to steps included in the DPoI, internal hard decoding and calculation of the prevailing distortion term, $d(n) = y(n) - x(n)$, are also included in each PANC iteration [6], requiring $2MN_{act}$ *mul*s and $3MN_{act}$ *add*s for M–QAM modulation, and $2N$ real *add*s.

A numerical example with $N_{\text{act}} = 3168$, $N_{\text{FFT}} = 4096$, $\varepsilon = 5$, $M = 64$, $P_{\text{RX}} = 7$, $D_{\text{RX}} = 4$ and 4 iterations of PANC results in DPoI complexity of 4.5×10^6 *mul*s and 3.7×10^6 *add*s, while the corresponding complexity of PANC is 19.8×10^6 *mul*s and 17.3×10^6 *add*s. These numbers highlight the complexity advantage of the DPoI compared to PANC.

III. RF Measurement Results

The proposed DPoI method is evaluated with 5G NR standard-compliant CP-OFDM waveforms of length 14 OFDM symbols (1 slot). The PAPR of the PDSCH symbols is limited to 8 dB with a soft envelope limiter, while the boosting of the DMRS is adopted as described in Section II.C. Also PANC [6] is implemented as a reference method where the nonlinear model coefficients are estimated at the receiver with the same LS approach described in Section II.C – except that now $x_{\text{ref}}(n)$ and $q_{\text{ref}}(n)$ are interchanged. This is because PANC uses a forward model of the TX nonlinearity [6]. Both 64-QAM and 256-QAM data modulations are considered for the PDSCH, with representative thermal noise SNRs of 20 dB and 25 dB, respectively. With double-DMRS configuration, the DMRS is contained in the 3rd and 4th OFDM symbols within each slot while in the single-DMRS case, it contains only the 3rd OFDM symbol. The actual DPoD methods with $P_{\text{RX}} = 7$ and $D_{\text{RX}} = 4$ are implemented on a host PC using MATLAB. Channel estimation is based on LMMSE processing.

The FR2 OTA measurement setup is shown in Fig. 3 where transmit signal with $\Delta f = 60$ kHz and $N_{\text{FFT}} = 4096$ is considered reflecting 200 MHz mmWave channel bandwidth case. Keysight M8190A arbitrary waveform generator (AWG) creates an IQ modulated transmit signal at 3.7 GHz intermediate frequency, which is then upconverted to 28.2 GHz with Marki Microwave T3-1040 mixer. Resulting RF signal is passed through Marki Microwave FB-3300 image filter and preamplified with two driver amplifiers – Analog Devices HMC499LC4 and HMC1131. Finally, the signal is fed into Anokiwave AWMF-0129 active antenna array, whose built-in amplifiers are the main source of nonlinear distortion. On the receiver side, the signal is captured by Pasternack PE9851A-20 horn antenna with 20 dB gain and digital samples are obtained with Keysight UXR0402AP oscilloscope.

Fig. 4 shows the measured receiver EVM values of the proposed DPoI and the reference PANC method (with 4 PANC iterations) with 64-QAM and single-DMRS configuration. It is observed that both methods provide significant EVM improvements while PANC is performing slightly better than DPoI. However, the computational complexity of DPoI ($4.5{\times}10^6$

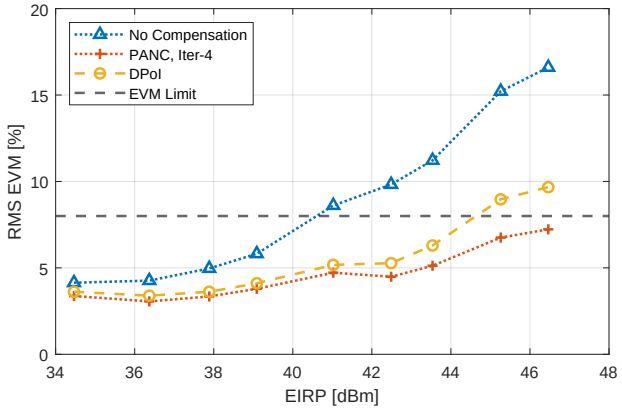

Fig. 4. FR2 active array measurement results at 28.2 GHz with 200 MHz bandwidth, 64-QAM data modulation and single-DMRS configuration.

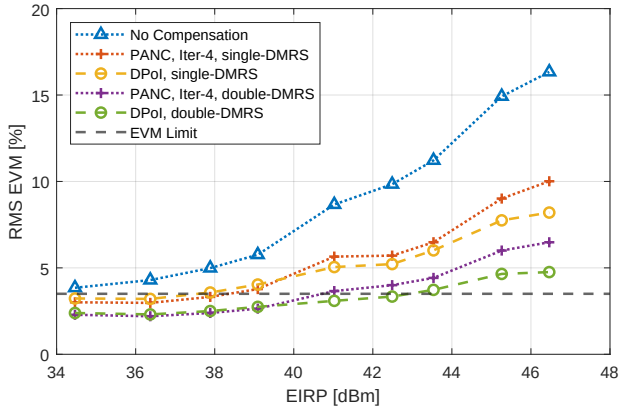

Fig. 5. FR2 active array measurement results at 28.2 GHz with 200 MHz bandwidth, 256-QAM data modulation and two DMRS configurations.

*mul*s and 3.7×10^6 *add*s) is significantly lower than that of PANC (19.8×10^6 *mul*s and 17.3×10^6 *add*s) when following the analysis principles given in Section II.D. Hence, DPoI can be considered more feasible for real-time UE implementations. It can also be observed that EIRPs up to around +45 dBm can be supported while still meeting the 8% EVM limit of 64-QAM, reflecting around 5 dB improvement compared to the no compensation case. This concretely highlights the benefit of DPoD processing from the radio link and EVM point of view.

Next, Fig. 5 shows the corresponding measured results with 256-QAM and when considering the single-DMRS and double-DMRS configurations, respectively. With the single-DMRS, we can observe that meeting the tight EVM limit of 3.5% standardized for 256-QAM is challenging. However, when two DMRS symbols are configured, the quality of the linear channel estimate as well as the accuracy of the nonlinear distortion model coefficients are both improved, and thus the EVM enhancement gains through DPoD processing are larger. Importantly, we can also observe that with the considered high modulation order, the proposed DPoI approach actually already outperforms PANC at the largest considered EIRP levels. This is because with very harsh nonlinearity at transmitter, the initial decisions utilized in the PANC iterative processing are already fairly unreliable. The proposed DPoI approach is, in turn, free from such limitations. Finally, the results in Fig. 5 show that meeting the EVM requirement of 3.5% is feasible up to EIRPs of around +42 dBm, when considering the proposed DPoI approach and double-DMRS configuration.

IV. Conclusions

In this paper, a computationally efficient digital post-distortion technique was presented and studied. Compared to the existing iterative methods, the proposed DPoI method is a one-shot approach, building on DMRS based linear channel and nonlinear model parameter estimates and the corresponding linear equalization and nonlinear post-inverse processing at the receiver. RF measurement results with an FR2 mmWave active array system showed comparable or improved performance compared to state-of-the-art iterative reference techniques, but with greatly reduced processing complexity. Especially with high modulation orders like 256-QAM and when transmitter is subject to harsh nonlinearities, the proposed DPoI method outperforms the reference iterative detection based nonlinearity cancellation schemes. As concrete outcomes, the DPoI method allows to increase the EIRP of the 28 GHz active antenna array by around 8–9 dB with 256-QAM, while still fulfilling the corresponding EVM limit of 3.5% at the receiver.

References

[1] C. Fager *et al.*, "Linearity and efficiency in 5G transmitters: New techniques for analyzing efficiency, linearity, and linearization in a 5G active antenna transmitter context," *IEEE Microw. Mag.*, vol. 20, no. 5, pp. 35–49, 2019.

[2] L. Guan and A. Zhu, "Green communications: Digital predistortion for wideband RF power amplifiers," *IEEE Microw. Mag.*, vol. 15, no. 7, pp. 84–99, 2014.

[3] Z. Alina and O. Amrani, "On digital post-distortion techniques," *IEEE Trans. Signal Process.*, vol. 64, no. 3, pp. 603–614, Feb. 2016.

[4] A. Brihuega *et al.*, "Piecewise digital predistortion for mmwave active antenna arrays: Algorithms and measurements," *IEEE Trans. Microw. Theory Techn.*, vol. 68, no. 9, pp. 4000–4017, Sep. 2020.

[5] 3GPP, "Study on network energy savings for NR (Release 18)," Technical Report (TR) 38.864, Dec. 2022, version 18.0.0.

[6] J. Tellado, L. Hoo, and J. Cioffi, "Maximum-likelihood detection of nonlinearly distorted multicarrier symbols by iterative decoding," *IEEE Trans. Commun.*, vol. 51, no. 2, pp. 218–228, Feb. 2003.

[7] J. Šterba, J. Gazda, M. Deumal, and D. Kocur, "Iterative algorithm for nonlinear noise cancellation and channel re-estimation in nonlinearly distorted OFDM system," in *Proc. IEEE SAMI*, Herlany, Slovakia, Jan. 28-30, 2010, pp. 65–70.

[8] F. Gregorio, S. Werner, T. I. Laakso, and J. Cousseau, "Receiver cancellation technique for nonlinear power amplifier distortion in SDMA–OFDM systems," *IEEE Trans. Veh. Technol.*, vol. 56, no. 5, pp. 2499–2516, Sep. 2007.

[9] F. H. Gregorio, S. Werner, J. E. Cousseau, and R. Wichman, "Broadband power amplifier distortion cancellation with model estimation in the receiver," in *Proc. IEEE SPAWC*, Helsinki, Finland, June 2007, pp. 1–5.

[10] H. Ku and J. Kenney, "Behavioral modeling of nonlinear RF power amplifiers considering memory effects," *IEEE Trans. Microw. Theory Techn.*, vol. 51, no. 12, pp. 2495–2504, Dec. 2003.

[11] K.-C. Hung and D. W. Lin, "Pilot-based LMMSE channel estimation for OFDM systems with power–delay profile approximation," *IEEE Trans. Veh. Technol.*, vol. 59, no. 1, pp. 150–159, Jan. 2010.

[12] D. Morgan, Z. Ma, and L. Ding, "Reducing measurement noise effects in digital predistortion of RF power amplifiers," in *Proc. IEEE ICC*, AK, USA, May 11-15, 2003, pp. 2436–2439.

[13] J. W. Cooley and J. W. Tukey, "An algorithm for the machine calculation of complex Fourier series," *Mathematics of Computation*, vol. 19, pp. 297–301, 1965.